Electrochimica Acta 146 (2014) 178–185

Contents lists available at ScienceDirect

Electrochimica Acta

journal homepage: www.elsevier.com/locate/electacta

Quaternized chitosan mediated assembly of gold nanoparticles multilayers

María V. Bracamonte, Omar E. Linárez Pérez, Manuel López Teijelo, Gustavo A. Rivas, Nancy F. Ferreyra *

INFIQC, Departamento de Fisicoquímica, Facultad de Ciencias Químicas, Universidad Nacional de Córdoba, 5000 Córdoba, Argentina

ARTICLE INFO

Article history:
Received 6 May 2014
Received in revised form 15 August 2014
Accepted 25 August 2014
Available online 18 September 2014

Keywords:
Self-assembled multilayers
Gold nanoparticles
Ellipsometry
Optical anisotropy
Electron transfer.

ABSTRACT

Self-assembled multilayers of quaternized chitosan (QCHI) and gold nanoparticles (AuNPs) were built up on quartz and gold substrates. To evaluate the effect of the surface coverage of AuNPs on the structural, optical and electrochemical properties of multilayers prepared with different AuNPs adsorption time were compared. UV-Vis and AFM characterization indicated that AuNPs in each bilayer are spatially separated, and interparticle interactions are mainly produced between bilayers. The complex refractive index and thickness of the QCHI-AuNPs multilayers were properly determined using an anisotropic single layer model. The optical constants obtained were quite different from those of bulk gold, and their values depend on the coverage of AuNPs. The thickness per bilayer of the structures present a progressive increase as AuNP's coverage augments, reaching a value close to the nominal AuNPs diameter after 60 min of adsorption. These results indicate that the interpenetration of bilayers in the structure depends on the surface concentration of AuNPs. The charge transport through the QCHI-AuNPs film was studied using different redox probes. The effects of the adsorption time of AuNPs and the number of bilayers (n) of the structure on the charge transfer rate constants, k_{ct}, were analyzed. The incorporation of AuNPs in the structure produces an increase of k_{ct}, as the adsorption time of AuNPs rise. In addition, the values of k_{ct} were independent of n, in the interval studied (up to n = 5), suggesting that the electronic communication in the multilayered structure was mediated by the AuNPs.

1. Introduction

Materials at the nanoscale have received significant attention in the last few decades because of their interesting and well-known properties associated with quantum confinement and surface energy effects [1]. Extensive research has been reported about synthesis [2], functionalization [3] and applications [4,5] of nanoparticles. Among the different types of metal nanoparticles, gold nanoparticles (AuNPs) have been extensively studied because their synthesis and functionalization is relatively simple and they exhibit excellent biocompatibility with biological components. These properties make AuNPs very attractive for their applications in sensors, electrocatalysis and medical diagnostic, among others [6]. In order to develop devices that exploit the properties of AuNPs, they should be anchored in a stable way on a surface, which often represents a critical step. In this sense, the construction of layer-by-layer (LbL) assembled structures with polymers is quite attractive because of its simplicity, flexibility and effectiveness [7,8]. The LbL method is well established in forming highly dense and compact ultrathin films using various kinds of organic or polymeric materials, with precise control of layer composition and thickness [9]. Multilayer thin films of gold nanoparticles linked with cationic polyelectrolytes such as poly(allylamine hydrochloride) (PAH) [10,11], polyethylenimine (PEI) [12], chitosan [13], modified chitosan [14], among others [15,16] have been reported. The morphology of these polymeric-AuNPs self-assembled structures depends on the environmental conditions, including pH, ionic strength, temperature, and nature of the ions and co-solvent of the adsorption medium [17].

AuNPs included in these self-assembled arrays present strong interactions with the matrix and neighboring AuNPs in the same layer (intralayer) as well as between layers (interlayer) [18]. These interactions generate collective surface plasmon resonances (SPR) controlled by the packing density and the interparticle distances along with the changing dielectric constant of interparticle media [19]. For example, Tsukruk and co-workers [20] have reported the

* Corresponding author. INFIQC, Departamento de Fisicoquímica, Facultad de Ciencias Químicas, Universidad Nacional de Córdoba, Ciudad Universitaria, 5000, Córdoba, Argentina; Tel.: +54 351 5353866 int. 53558; fax: +54 351 4334188.
E-mail addresses: ferreyra@fcq.unc.edu.ar, nfferreyra@gmail.com (N.F. Ferreyra).

http://dx.doi.org/10.1016/j.electacta.2014.08.109
0013-4686/

fabrication of LbL assembled films containing gold nanoparticles with control of the aggregation state by the design of multilayered films with various combinations of polymers interlayers [20]. Accordingly, assemblies of polymers/gold nanoparticles can be used to tune the optical properties providing a cheap and effective bottom-up approach for fabrication of plasmonic devices to develop sensors and biosensors systems [5].

In addition, electrode/polymer/nanoparticles assemblies present interesting electronic and catalytic properties. Understand the effect of the charge, size and density of nanoparticles, as well as the thickness of the structures on the efficiency of electron-transfer kinetics is required to exploit rationally the properties of these systems in sensing and electrocatalysis. Our main goal in this work is deepen on the relationship between the structural and electrochemical properties self assembled structures of gold nanoparticles. In a previous work [14] we evaluate the effect of quaternized quitosan (QCHI) and gold nanoparticles (AuNps) multilayer as platform for the adsorption of glucose oxidase (GOD) and we determine the influence of the AuNps in the enzymatic response of the biosensor. In relation with that work, in the present publication we extend our studies towards the structural and electrochemical characterization of QCHI/AuNps self assembled multilayers to correlate its physicochemical properties with the electrochemical response reported in ref. 14, such as the improvement of conductivity, the increment of the oxidation of the hydrogen peroxide produced by GOD, the higher amperometric response and the better analytical performance of electrodes modified with self assembled layers of QCHI/AuNps. For this purpose, in the present contribution we study the properties of self assembled multilayer films of quaternized chitosan (QCHI) and gold nanoparticles (AuNPs) to evaluate the influence of the surface coverage of nanoparticles, Γ_{AuNPs}, on the structural (thickness, distribution), and optical (refractive index, anisotropy) properties of the multilayers and correlate them with the electron-transfer kinetics at the modified electrode. QCHI/AuNPS multilayers were built up on quartz and gold substrates employing different AuNPs adsorption time. The systems were characterized using optical (UV-Vis, ellipsometry), microscopic (AFM, TEM, SEM) and electrochemical techniques (CV, EDR, EIS) and the evolution of the complex refractive index and thickness of each structure were evaluated as a function of Γ_{AuNPs}. The heterogeneous charge transfer rate constants of different redox probes were determined varying two parameters, the adsorption time of nanoparticles or the number of bilayers of chitosan/nanoparticles. The results presented in this contribution evidence that the adsorption of AuNPs improves the conductivity of the structure as well as its electrochemical reactivity. Both characteristics depend, in turn, on the structural properties of the chitosan/AuNPs arrays.

2. Experimental section

2.1. Reagents

Citrate-stabilized gold nanoparticles (AuNPs) with λ_{max} = 518 nm, (11.0 ± 0.7) nm average diameter and 3.72 x 10^{12} nanoparticles mL^{-1} were from Sigma. The average size of AuNPs was confirmed by transmission electron microscopy, see supporting information S1. The sodium salt 3-mercapto-1-propanesulfonate (MPS) was obtained from Aldrich. Quaternized chitosan (QCHI) was synthesized as described in reference [21] from chitosan of 190 kDa molecular weight (Pronova). The average molecular weight of QCHI was 52.75 kDa and the content of quaternized amine 40.0 mol %. Other chemicals were of reagent grade and were used without further purification. All solutions were prepared with ultra-pure water (18 MΩ cm) from a Millipore-MilliQ system.

2.2. Equipments

UV-Vis experiments were performed with a Shimadzu UV1601 Spectrophotometer and a quartz cuvette with a 0.1 cm path length. Atomic force microscopy (AFM) images were obtained with a Multiview 1000 Nanonics Microscope using a cantilevered optical fiber probe of 10 nm of diameter coated with Al. Images were collected in air using intermittent mode and processed with the WSXM software [22]. Scanning electron microscopy (SEM) images were obtained with a Field Emission Gun Scanning Electron Microscope (FE-SEM, Zeiss, ΣIGMA model). Ellipsometric experiments were performed with a Rudolf Research rotating analyzer automatic ellipsometer (vertical type, 2000FT model), equipped with a 75 W tungsten lamp as the light source and filters (632.8 and 546.1 nm). All measurements were performed at an incidence angle of 70.00°. A homemade gold electrode of 7 mm of diameter was used as substrate. The gold electrode was horizontally mounted in a Teflon holder and aligned before each experiment. The adsorption of QCHI and AuNPs was carried out without variations of the substrate position to keep the system alignment. The ellipsometric angles (Ψ and Δ) were collected in 5.00 x 10^{-2} mol dm^{-3} phosphate buffer solution pH 7.40 after each adsorption step. The operator-triggered mode was employed for taking the measurements. Cyclic voltammetry (CV) was performed with a 173 EG&G PAR potentiostat/galvanostat (Princeton Applied Research, USA) coupled to a 175 EG&G PAR signal generator and a 7090A Hewlett Packard plotting recorder. Stationary potential/current curves were obtained at a gold rotating disk electrode (Radiometer Analytical, EDI101) using a rotation speed controller (Radiometer Analytical, CTV101). Electrochemical impedance spectroscopy (EIS) experiments were performed with a Solartron potentiostat/galvanostat (SI 1287) coupled to a frequency response analyzer Solartron FRA 1260. Measurements were performed at the open circuit potential with a 10 mV of amplitude signal in the frequency interval from 10 mHz to 0.1 MHz was applied. Gold disk electrodes (Au) of 2 mm diameter (CHI 101) were used as substrate during the electrochemical experiments. A platinum wire and an Ag/AgCl/3 mol dm^{-3} NaCl electrode (Model RE-5B, BAS) were used as counter and reference electrodes, respectively. The reported potentials are referred to this reference electrode. All experiments were performed at room temperature.

2.3. Surface Modification

2.3.1. Gold modification

Gold electrodes were cleaned before each experiment by polishing for 6 min with 0.05 μm alumina, followed by sonication in deionized water for 5 min, immersion in "Piranha" solution (1:3 V/V H_2O_2/H_2SO_4) for 5 min, and rinsing with ultrapure water. The surfaces were stabilized by cycling at 10 V s^{-1} of scan rate in 0.50 mol dm^{-3} sulphuric acid solution between 0.200 V and 1.650 V until a reproducible voltammogram corresponding to a clean gold surface was obtained. To check the surface condition and to obtain the electro-active area, a voltammogram in 0.50 mol dm^{-3} sulphuric acid solution at 0.100 V s^{-1} was performed at the end of the cleaning procedure.

ArrandeeTM glass slides of 11 x 11 mm covered with a gold deposit were used as substrates for AFM and SEM experiments. To promote the development of Au (111) planes, the substrates were annealed in a butane flame during two minutes, cooled under constant N_2 flux and placed immediately in the dipping solution.

The first step in the preparation of the multilayer was the adsorption of MPS by soaking the substrates for 30 min in 2.00 × 10^{-2} mol dm^{-3} MPS solution prepared in 1.6 × 10^{-3} mol dm^{-3} sulphuric acid solution, followed by a careful rinsing with deionized water. The adsorption of QCHI was performed for 20 min from a 0.50 mg mL^{-1} QCHI solution prepared in 5.00 x 10^{-2} mol

dm^{-3} phosphate buffer solution pH 7.40. The conditions for the adsorption of MPS and QCHI were optimized in previous studies [14]. The adsorption of AuNPs was performed by immersion of Au/MPS/QCHI surfaces in the colloidal solution for a given time. After each adsorption step, surfaces were copiously rinsed with 5.00 x 10^{-2} mol dm^{-3} phosphate buffer solution pH 7.40. Multilayered films were constructed by alternate immersion of Au/MPS substrates in QCHI and AuNPs solutions. The resulting surfaces are indicated as Au/MPS/$(QCHI\text{-}AuNPs)_n$, with n being the number of QCHI-AuNPs bilayers.

2.3.2. Quartz modification

In order to expose negative charges, the internal surface of a quartz cuvette, Q, was sonicated in ethanolic solution of NaOH 1.0% W/V for 20 min. Adsorption of QCHI and AuNPs was performed filling the cuvette with each solution for a given time. Then, the solutions were removed, and the cuvette was repeatedly washed with 5.00 x 10^{-2} mol dm^{-3} phosphate buffer solution pH 7.40. The resulting structure with the desired number of bilayers is indicated as $Q/(QCHI\text{-}AuNPs)_n$. In all cases the baseline and spectral curves were obtained in 5.00 x 10^{-2} mol dm^{-3} phosphate buffer solution pH 7.40.

2.4. Fundamentals of Ellipsometry

Ellipsometry is a method widely used to study the characteristics of thin films onto modified surfaces [23–25]. This technique measures the change in polarization state of light reflected from the surface of a sample in terms of the ellipsometric angles Ψ and Δ [26].

The values of the ellipsometric angles Ψ and Δ cannot be directly converted into the refraction index and thickness depth profile of the film, rather, a model-based iterative procedure is used to fit the experimentally measured Ψ and Δ values. In the present paper, we used a single-layer film model with anisotropic optical properties (ASLM) to analyze Ψ-Δ evolution during the construction of (QCHI-AuNPs) multilayers at Au/MPS. The experimental data were fitted using the Simplex method [27]. From the fitting procedure, the complex refractive index, written in terms of its real part, n (refractive index), and imaginary part, k (extinction coefficient), as $\check{n} = n - i\,k$ [26] were obtained. The optical constants of parallel (extraordinary) and perpendicular (ordinary) direction, referred as n_{or}, k_{or}, n_{ext} and k_{ext}, as well as the thickness for each experimental point, were determined [23].

3. Results and discussion

3.1. UV-Vis characterization

Fig. 1 shows the UV-Vis spectra of Q/QCHI (dashed lines) and Q/(QCHI-AuNPs) (solid lines), obtained by increasing the contact time of the colloidal solution with the surface from 15 to 120 min. After the adsorption of AuNPs, one broad band is observed that corresponds to the SPR of the AuNPs [28]. In comparison with AuNPs in solution, the adsorption on the polymer produces a red-shift of 7 nm as consequence of the difference of the dielectric constant of both medium. By other way, λ_{max} presents also a progressive red-shift from 525 nm (15 min) up to 545 nm at 60 min. This shift is a consequence of the variation on the dielectric constant of the medium and can be explained by the Effective Medium Theory [29]. AuNps are embedded in a matrix and are therefore subject to average polarization field due to the matrix and the particles, and the factor responsible for the red-shift is the volume fraction of gold nanoparticles included in the medium that depends on the AuNps adsorption time.

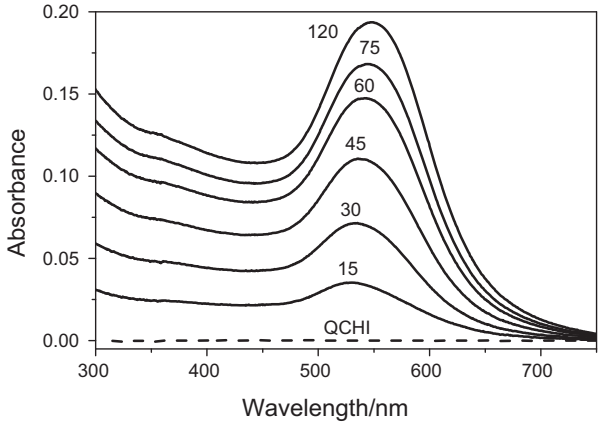

Fig. 1. Spectral curves of (—) Q/QCHI and (—) Q/(QCHI-AuNPs) obtained with increasing AuNPs adsorption time from 15 min to 120 min.

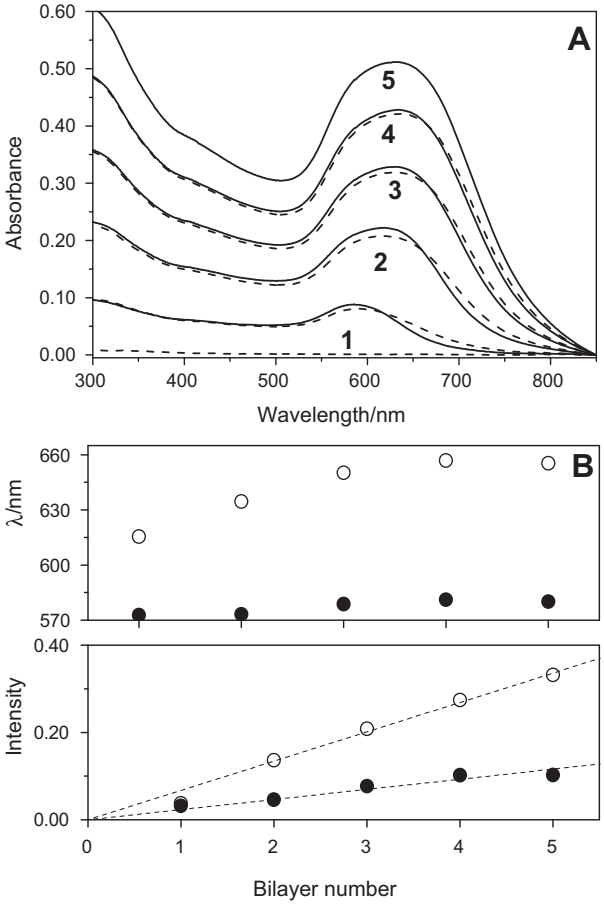

Fig. 2. A) Spectral curves of Q/(QCHI-AuNPs)n structures built with one to five bilayers, (—) QCHI external layer and (–) AuNPs external layer. B) Variation of the SPR positions and intensity of SPR band of individual nanoparticles (●) and the collective resonances (○) as a function of the bilayer number, n. Measures were performed in 0.100 mol dm^{-3} phosphate buffer solution pH 7.40. Adsorption time: 20 min for QCHI and 60 min for AuNPs.

The plot of the maximal absorbance (Abs_{max}) versus the square root of the adsorption time presents a good linear relationship ($R^2 = 0.996$) up to 90 min, which indicates that AuNPs adsorption on Q/QCHI surface follows a diffusion-controlled kinetics in the early stages [28], (Figure S2 of supporting information).

For the multilayer construction, 20 min and 60 min of adsorption time were selected for QCHI and AuNPs, respectively. Fig. 2A

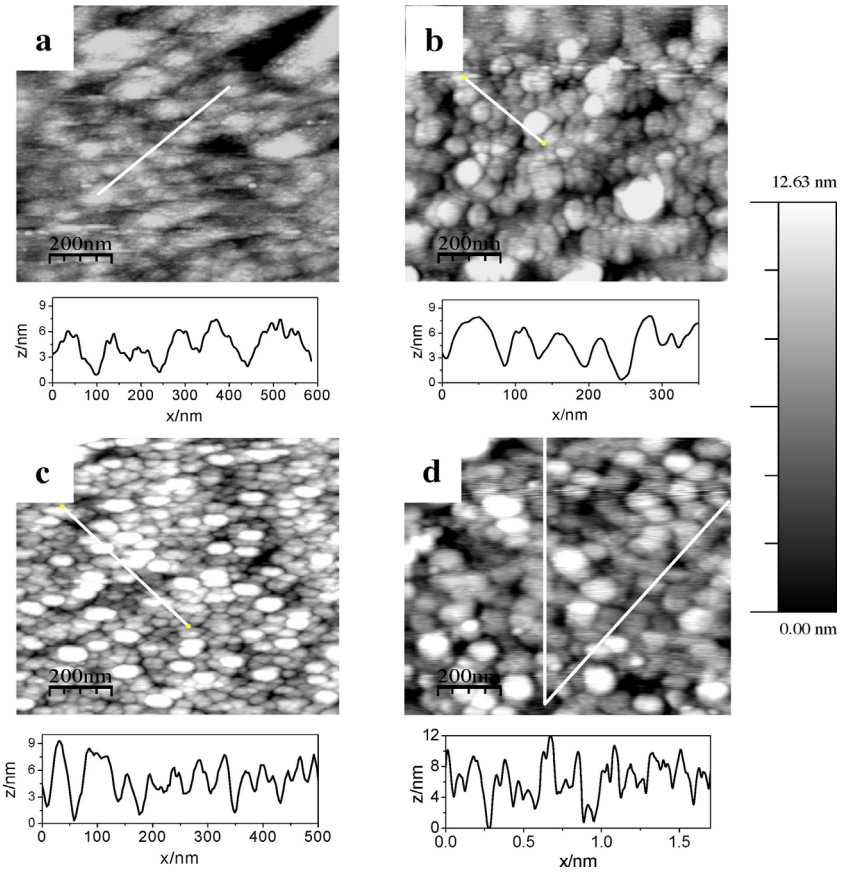

Fig. 3. A) AFM images and cross-section plots of Au/MPS/(QCHI-AuNPs) surfaces modified with (a) 15 min, (b) 30 min and (c) 60 min of AuNPs adsorption time and (d) Au/MPS/$(QCHI\text{-}AuNPs)_2$ surface built with 30 min of AuNPs adsorption.

shows UV-visible absorption spectra of Q/$(QCHI\text{-}AuNPs)_n$ multilayers with 1 to 5 bilayers, dashed lines correspond to structures ended in QCHI and solid lines to those ended in AuNPs. Clearly, the extinction increases with the number of bilayers, being this effect associated to the increment of AuNPs adsorbed. In addition, a widening of the bands is also observed. To evaluate this point, the spectra were analyzed following the procedure described by Schiffrin and coworkers [30], which consider two main contributions: the SPR band that could be attributed to individual nanoparticles and the collective resonances due to interactions between closer nanoparticles (Figure S3 of supporting information). Fig. 2B presents the variation of the intensity and position of both contributions as a function of n. The intensity for each contribution, evaluated at the corresponding value of λ_{max}, increases linearly with the number of bilayers, indicating that the amount of AuNPs adsorbed during each adsorption cycle is constant. Due to the surface coverage of AuNPs is mainly dependent on the coverage of QCHI, these results indicate a good reproducibility of the alternate adsorption methodology of QCHI and AuNPs. The position of the band at 570 nm is almost constant, while the corresponding to the inter-particle resonances shifts up to 660 nm as n increases. Similar results have been reported for AuNPs in self-assembled multilayers with the polycation PEI and PAH [12,20], and were attributed to interactions between neighboring particles that produce a red shift of λ_{max}.

3.2. Microscopic characterization

The surface morphology of Au/MPS/$(QCHI\text{-}AuNPs)_n$ structures was examined by AFM. Fig. 3 shows the images and cross section plots of one bilayer varying the AuNPs adsorption time. A homogeneous distribution of AuNPs at the modified substrate and a decrease of uncovered areas are observed as the adsorption time of AuNPs increases. The average heights are 6.5 nm, 6.5 nm and 8.0 nm for the images (a), (b) and (c), respectively, while the root-mean-square roughness (rms) are 2.5 nm, 2.9 nm, and 3.4 nm, respectively. Height and rms values of Au/MPS/QCHI structures were 5.5 nm and 1.7 nm, respectively. From these results it can be conclude that AuNPs are embedded in a rough layer of QCHI, and the empty zones of the modified surface are gradually covered as the AuNPs adsorption time increases. Despite of the images a to c present well-defined boundaries between neighboring AuNPs, the xy plane and the cross section plots show significant higher dimensions of AuNPs compared to its average diameter. This is a common AFM artifact associated with tip dilation of lateral dimensions of nanoscale objects [31] and could lead to estimate an artificially higher value of AuNPs surface concentration making difficult to determine quantitatively the surface density of AuNPs [20]. To complement the AFM analysis and to evaluate the distribution of AuNps without the effect of enlarged lateral dimension, SEM images were also obtained (Figure S4 of SI). In the micrograph, isolated AuNPs are seen as bright spots and it is evident that low coverage and homogeneous distribution of AuNPs are obtained, indicating the absence of AuNPs aggregation.

The height and rms of Au/MPS/$(QCHI\text{-}AuNPs)_n$ multilayers built using 30 min of AuNPs adsorption time were also determined. Fig. 3 (d) shows the image for the adsorption of two bilayers. The heights obtained for structures with one, two and three bilayers of QCHI-AuNPs were 6.5 nm, 8 nm and 10 nm while the rms were 2.9 nm, 3.1 nm and 5.0 nm, respectively. The height and roughness increase

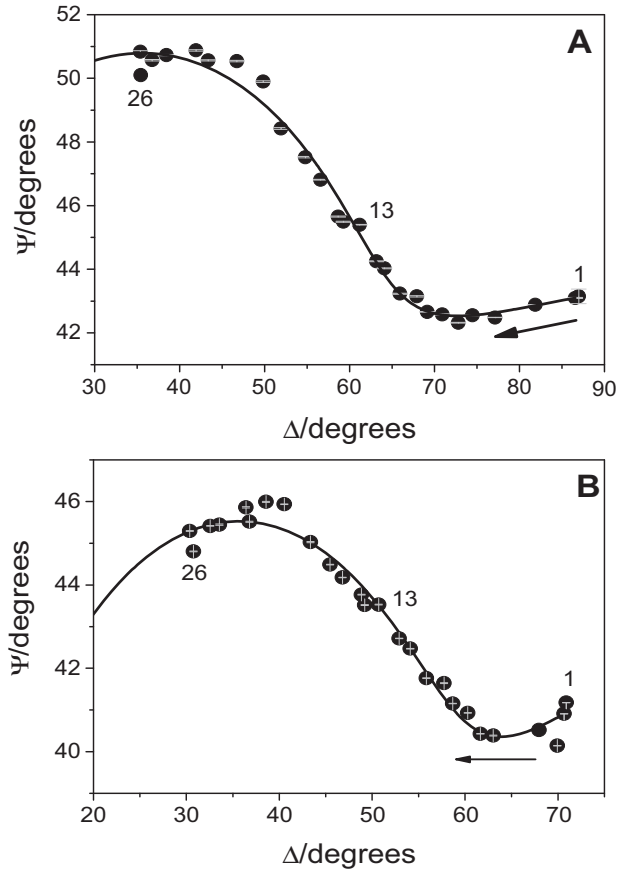

Fig. 4. Ψ-Δ plots obtained at **A)** 632.8 nm and **B)** 546.1 nm during the assembled of $(QCHI\text{-}AuNPs)_n$ multilayer at Au/MPS surface; (●) experimental points and (—) best fit obtained with the anisotropic single layer model. The arrows indicate the direction of the thickness increase. Electrolyte: 0.100 mol dm^{-3} phosphate buffer solution pH 7.40. Adsorption time: 20 min for QCHI and 30 min for AuNPs.

with the number of bilayers, but the increment of height is lower than the diameter of AuNPs, indicating that bilayers are interpenetrated.

3.3. Ellipsometric characterization

The optical characteristics of self-assembled structures are strongly dependent on the adsorption conditions of AuNPs. Ellipsometric response (Ψ and Δ) is very sensitive to changes in the surface morphology, thickness, and refractive index of the sample. Consequently, variations of the complex refractive indices for different AuNPs surface concentrations are expected [32,33]. We evaluate the optical properties and thickness of $(QCHI\text{-}AuNPs)_n$ multilayers prepared with 15 min, 30 min and 60 min of AuNPs adsorption time. For each adsorption time of AuNps, the variation of Ψ-Δ angles during the assembly construction were measured at two different wavelengths, 632.8 nm and 546.1 nm. Then, each plot was fitted considering a simple layer model and the optical parameters and thickness of the film were obtained. As the thickness is a property of the film, measurements at two different wavelengths and their corresponding fits allowed us evaluating the correctness of the determined thickness and to calculate average values.

Fig. 4 shows the Ψ-Δ evolution during the step-by-step assembly of QCHI-AuNPs multilayer on Au/MPS surface at (A) 632.8 nm and (B) 546.1 nm. The nanoparticles were adsorbed for 30 min and the measurements were done in 5.00 x 10^{-2} mol dm^{-3} phosphate buffer solution pH 7.40. Each symbol corresponds to the experimental value of the bilayers 1 to 26 for the structure ended

Table 1
Optical parameters of $Au/MPS/(QCHI\text{-}AuNPs)_n$ structure prepared with 30 min of AuNPs adsorption time.

Optical[a] parameter	n_{or}	k_{or}	n_{ext}	k_{ext}
632.8 nm	1.595	0.415	2.290	~ 0
546.1 nm	1.646	0.471	1.919	0.241

[a] Fits with ASLM. Optical parameters for the solvent were $n_o = 1.333$ and $k_o = 0.000$.

in AuNPs, the line is the calculated curve with the parameters obtained from the best fitting obtained with the ASLM. The good agreement between the calculated curves and the experimental Ψ-Δ data validates the ASLM proposed and allowed us to obtain accurate values of n and k for normal and parallel directions to the surface. Table 1 summarizes the optical parameters obtained at 632.8 nm and 546.1 nm. The complex refractive indices at both wavelengths are quite different from that of bulk gold ($\check{n} = 0.197 - i3.45$ at 633 nm) [15]. This notorious variation is attributed to the low Γ_{AuNPs} of the structures studied. The difference between $\check{n}_{ord}$ and $\check{n}_{ext}$ determined at both wavelengths as well as the values significantly high of k_{ord} indicates that the interparticle interactions in the vertical direction (i.e., the out-of-plane interactions) are different from those in the lateral direction (i.e., the in-plane interactions), producing the optical anisotropy of the film. The relatively high values of the extinction coefficients are in agreement with the SPR position band in the UV-Vis experiments. Anisotropic properties of polymers/AuNPs multilayers have been previously reported by Z. Qi et al. for multilayer thin films of gold nanoparticles and the protein myoglobin (AuNPs/Mb) [34]. Under the experimental conditions employed for the authors, very weak out-of plane interactions between NPs of different layers was observed, ascribed to the limited numbers of NPs/Mb bilayers. The authors also indicated that closely packed multilayer films with higher number of NPs layers could enhance the out-of plane interactions, and finally make the film optically anisotropic [34].

Optical properties and thickness of (QCHI-AuNPs)n multilayers prepared with 15 min, and 60 min of AuNPs adsorption time were also evaluated. Fig. 5 shows the Ψ-Δ plots of $Au/MPS/(QCHI\text{-}AuNPs)_n$ multilayers for 60 min of AuNPs measured at 632.8 nm. From the fit we determined the complex refractive indexes, $\check{n}_{ord} = 1.427 - i\ 0.416$ and $\check{n}_{ext} = 2.913 - i\ 0.178$. Form the the same analysis performed with 15 min of AuNps adsorption time (not shown) we determined $\check{n}_{ord} = 1.375 - i\ 0.041$ and $\check{n}_{ext} = 1.612 - i\ 0.00$. From the comparison of the results obtained at 15, 30 and 60 min is clear that as Γ_{AuNPs} increases, a rise of the extinction coefficient

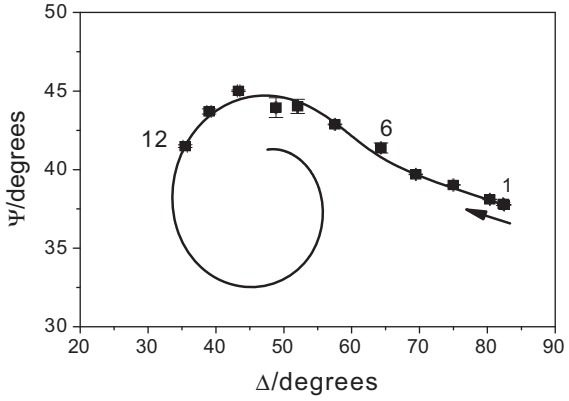

Fig. 5. Ψ-Δ plots obtained at 632.8 nm during the assembled of $(QCHI\text{-}AuNPs)_n$ multilayer at Au/MPS surface with 60 min of AuNps adsorption time; (●) experimental points and (—) best fit obtained with the anisotropic single layer model. The arrows indicate the direction of the thickness increase. Electrolyte: 0.100 mol dm^{-3} phosphate buffer solution pH 7.40. Adsorption time: 20 min for QCHI and 30 min for AuNPs.

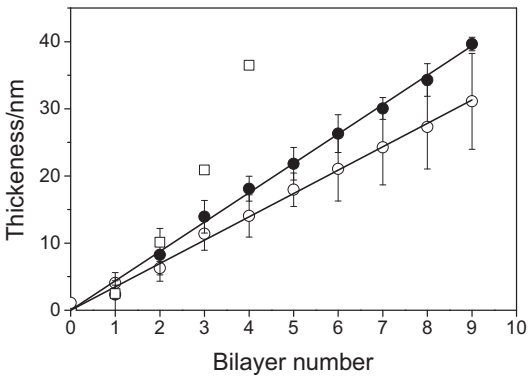

Fig. 6. Evolution of the average thickness determined from measurements at 546.1 and 632.8 nm as a function of the bilayer number of structures built using (○) 15 min, (●) 30 min and (□) 60 min of AuNPs adsorption time; (–) linear fit of the experimental results.

and refractive index is observed, being more evident the effect in n_{ext}. The increase of the extinction coefficient can be understood considering the variation of the intensity and position of the SPR absorption band [32]. The increase of k value at 632.8 nm is attributed mainly to interparticle interactions, which are favored as Γ_{AuNPs} increases. The values obtained are comparable to those reported by E. S. Kooij et al. for AuNPs self-assembled [33] and multilayers of AuNPs and the protein myoglobin, $\check{n}_{or} = 1.702 - i\ 0.43$ [34], systems with low surface coverage of AuNPs.

Additionally, from the fitting procedure, the bilayer thicknesses were obtained. Fig. 6 shows the average thickness determined from the measurements at 546.1 and 632.8 nm as a function of the numbers of bilayers of structures built using 15 and 30 min of AuNPs adsorption time. Both sets of data evidenced a linear thickness growth. However, the mean thickness per layer is 3.0 nm and 4.5 nm for the multilayers built using 15 min and 30 min of AuNPs adsorption time, respectively. Because of the AuNPs nominal diameter is (11.0 ± 0.7) nm, these results clearly indicate the occurrence of a pronounced interpenetration of layers, in agreement with the conclusions obtained in section 3.2. This effect is more evident when the structures are built with lower AuNPs surface coverage (shorter adsorption times). The adsorption of AuNPs on the polymer layer leaves empty spaces available for adsorption of more AuNPs during the following bilayer deposition. This effect has been also demonstrated by A. Dobrynin et al using dynamic simulation [35]. As the adsorption time increases, the Γ_{AuNPs} per layer augment and the density of the empty spaces decreases. Under saturation conditions, the interpenetration of bilayers is reduced and the mean thickness per layer could reach a value close to the AuNPs diameter. In agreement with this tendency, experiments performed using 60 min of AuNPs adsorption time allowed us to determine an average thickness increase of around 10 nm per bilayer (squared symbols in fig. 6).

3.4. Electrochemical characterization

The electrochemical response of $K_3[Fe(CN)_6]/K_4[Fe(CN)_6]$ and ferrocene methanol (FcMOH) redox probes at different surfaces was studied. Cyclic voltammetry (CV), rotating disk electrode (RDE) and EIS were used to evaluate the effect of Γ_{AuNPs} on the charge transfer process and the electrochemical response as a function of the number of adsorbed bilayers and to complement and verify the results previously reported in 14.

Fig. 7A shows the Nyquist plots obtained at Au/MPS, Au/MPS/QCHI and Au/MPS/QCHI-AuNPs with different AuNPs adsorption time. Measurements were performed in the presence of 1.00 x 10^{-3} mol dm^{-3} equimolar solution of $K_3[Fe(CN)_6]/K_4[Fe(CN)_6]$ prepared in 5.00 x 10^{-2} mol dm^{-3} phosphate buffer solution pH = 7.40. The spectra were fitted using the Randles circuit presented in the inset, were Rs, W, R_{ct}, C_{dl} are the solution resistance, the Warburg impedance, the charge transfer resistance and the double layer capacity, respectively. Compared to bare gold (not shown), the resistance increases when MPS is adsorbed due to the negative charges of the sulfonate groups. On the contrary, the assembly of QCHI produces a decrease of R_{ct} due to the electrostatic attraction between the polycation and the negatively charged redox probe. After the adsorption of the citrate stabilized AuNPs, an increase of R_{ct} is observed as the adsorption time of the particles augment. This effect is produced by the negative charges exposed on the surface that repels the redox couple [36]. Fig. 7B shows the values of R_{ct} of $(QCHI\text{-}AuNPs)_n$ multilayers determined from experiments performed in phosphate buffer solution pH 7.40 with ionic strength 0.1 (empty symbols) and 0.2 (full symbols). In the first case, the reversion of charge produced at the electrode surface after the adsorption of the polycation and the anionic AuNPs is evidenced in the zigzag response of R_{ct} observed during the alternative immobilization of QCHI and AuNPs layers. Under high ionic strength, the ions of the supporting electrolyte produce external charge compensation and reduce the electrostatic repulsion between the modified surface and the redox probe. Consequently, a smooth variation of R_{ct} is observed during the alternate adsorption of the polycation

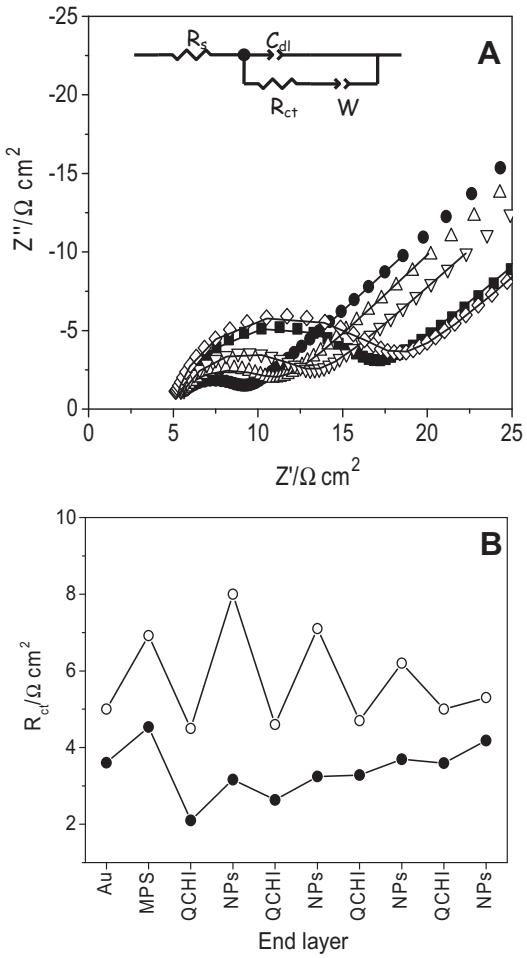

Fig. 7. A) Nyquist plot obtained at (■) Au/MPS; (●) Au/MPS/QCHI and $Au/MPS/(QCHI\text{-}AuNPs)_1$ built with (△) 15 min; (▽) 30 min and 60 min (◊) of AuNPs adsorption time. The inset shows the circuit used for fit. B) Variation of R_{ct} as a function of the end assembled layer. Experimental conditions: 1.0 x 10^{-3} mol dm^{-3} $K_3[Fe(CN)_6]/K_4[Fe(CN)_6]$ equimolar solution prepared in phosphate buffer pH 7.40 ionic strength (○) 0.1 and (●) 0.2.

Table 2
Charge transfer constants of $K_4[Fe(CN)_6]$ determined from EDR experiments.

Surface		k_{ct}[a]/10^{-2} cm s^{-1}
Au		0.7
Au/MPS		0.4
Au/MPS/QCHI		0.01
Au/MPS/(QCHI-AuNPs)	15 min[b]	0.08
	60 min[b]	1.4
	120 min[b]	3.0

Experimental conditions: [a]1.00 x 10^{-3} mol dm^{-3} $K_4[Fe(CN)_6]$ prepared in 0.500 mol dm^{-3} Na_2SO_4 solution. [b]AuNPs adsorption time.

and AuNPs, and the resistance remains practically constant as the number of bilayers increases.

In order to analyze the effect of AuNPs on the charge transference rate of $[Fe(CN)_6]^{3-}$ and FcMOH, RDE experiments we performed under high ionic strength conditions. The heterogeneous charge transfer constants, k_{ct}, were determined at bare gold and after the adsorption of MPS, QCHI and AuNPs (see figure S5 of supporting information). The values of k_{ct} for $[Fe(CN)_6]^{3-}$ calculated from the Tafel's plots [37] are presented in Table 2. The tendency observed for $[Fe(CN)_6]^{3-}$ is in agreement with reported results for FcMOH in our previous work [14]. Besides, in order to validate the results, cyclic voltammograms using the calculated values of k_{ct} of FcMOH [14], were simulated. From the simulations, (Figure S6 A to C of supporting information), theoretical values of peak potential separation, ΔEp_{theor}, were obtained and compared with experimental results, ΔEp_{exp}, from cyclic voltammetry experiments. A good correlation between both values was observed verifying the values of k_{ct}. From the analysis of the results obtained with both redox couples, it is clear that, regardless of charge and hydrophobicity of the redox probe, the adsorption of AuNPs produces an increase of $k_{ct.}$ The values of k_{ct} are also dependent on the Γ_{AuNPs}.

The electrochemical response reported here and in reference 14 are in agreement with the theory of Chazalviel and Allongue recently report that describes theoretically a mechanism for the nanoparticle-mediated electron transfer [38]. The theory suggested that effective nanoparticle-mediated electron transfer is expected, with distant independent rate of electron transfer, as long as exchange current density across an organic layer (OL) on the metal/OL/metal (J_1) assembly is much larger than that on a metal/OL (J_0) assembly. The theory was applied to OL of self assembled monolayers (SAMs) of of alkane thiols and not conductive polymer layers. The higher current density, J_1, is attributed to the high density of states on the other metal, to which the potential is not applied, in this case the nanoparticle. More recently, Gooding and coworkers evaluated experimentally the theory and determined the thickness of the OL beyond nanoparticle-mediated electron transfer is expected to be affected [39,40].

The efficient AuNPs-mediated electron transfer (ET) of Au/QCHI-AuNPs electrodes is in agreement with the theory and explains the improvement of conductivity and the increment of the oxidation of the hydrogen peroxide reported in reference 14. As consequence, the electrodes modified with self assembled layers of (QCHI/AuNPs) as platform for the adsorption of GOD presentedhigher amperometric response and the better analytical performance than electrodes without AuNPs [14].

The electrochemical response of FcMOH on self-assembled $Au/MPS/(QCHI\text{-}AuNPs)_n$ structures built with 60 min of AuNPs adsorption time was also analyzed to evaluate the ET at the multilayer. No variations of the peak current and ΔEp_{exp} and ipa values were observed as the number of bilayers n of (QCHI-AuNPs) increases at least in the range analyzed n = 5 (Figures S7 of supporting information). Using ΔEp_{exp} values, cyclic voltammograms were simulated and a value of $k_{ct} \sim 2 \times 10^{-2}$ cm s^{-1} was determined, (Figures S8 of supporting information). Considering that under the experimental conditions used the successful construction of the multilayers has been demonstrated by UV-Vis spectroscopy and ellipsometry, and the thickness increase was determined, the charge transfer should occur via a nanoparticle-mediated pathway. In an opposite way, a decrease of peak current and an increment of ΔEp_{exp} should be expected as the thickness of the structure increases. Because k_{ct} for FcMOH is independent of the multilayer thickness and is similar to the value determined at Au, we conclude that AuNPs acts as channels that favor the electronic conduction through the multilayer [41]. Similar results were also obtained with $K_3[Fe(CN)_6]$ (not shown). These results suggest that the intra or interlayer interaction of AuNPs promotes the electronic conduction between the AuNPs and the electrode surface, in agreement with previous reports of polyelectrolytes/AuNPs systems [42–44].

4. Conclusions

Multilayer films containing citrate-stabilized gold nanoparticles and QCHI were built on quartz and MPS-functionalized gold substrates. A diffusion-controlled process is observed in the early stages of AuNPs adsorption on the QCHI-modified surface. UV-Vis and AFM characterization indicated that AuNPs in each bilayer were spatially separated between them. The interparticle interactions were mainly produced between bilayers as a result of the interpenetration of the structure. The surface coverage and the coupling between particles depend on the adsorption time of AuNPs. The refractive indices for the (QCHI-AuNPs)n multilayers were properly determined using an anisotropic single layer model. The optical constants were quite different from those of bulk gold and their values vary with the AuNPs surface coverage. The thickness per bilayer of the structures present a progressive increase as Γ_{AuNPs} augments, reaching a value close to the nominal nanoparticles diameter after 60 min of adsorption. These results indicate that the interpenetration of bilayers in the multilayer depends on $\Gamma_{AuNPs.}$

The incorporation of AuNPs in the structure produces an increase of the heterogeneous charge transfer rate constant of redox probes and their values were dependent on the $\Gamma_{AuNPs.}$ The efficient AuNPs-mediated ET at Au/QCHI-AuNPs electrodes explains the improvement of conductivity and the increment of the oxidation of the hydrogen peroxide reported in reference 14. The electrodes modified with (QCHI/AuNPs) as platform for the adsorption of GOD presented higher amperometric response and a better analytical performance than electrodes without AuNPs. In relation to the multilayers, the kinetic constant of the charge transfer process was independent of the number of bilayers of QCHI-AuNPs, (in the range studied up to n = 5), and similar to the value determined at Au. These results indicate that the electronic conduction through the multilayer should be mediated by the AuNPs and favored by their distribution in the structure making evident that polymer/nanoparticles assemblies represents an important strategy for develop of electrochemical sensors and a biosensors.

Acknowledgment

The authors thank CONICET, SECyT-UNC and Agencia Nacional de Promoción Científica y Tecnológica (ANPCYT) for the financial support. M. V. Bracamonte thanks CONICET for the fellowship. The authors also thank to Prof. Pierre Labbé for academic contributions and Dr. Jacques Desbrieres for the synthesis of quaternized chitosan.

Appendix A. Supplementary data

Supplementary material related to this article can be found, in the online version, at http://dx.doi.org/10.1016/j.electacta.2014.08.109.

References

[1] R.M. Iost, F.N. Crespilho, Layer-by-layer self-assembly and electrochemistry: Applications in biosensing and bioelectronics, Biosens. Bioelectron. (2012) 1–10.
[2] S. Guo, E. Wang, Noble metal nanomaterials: Controllable synthesis and application in fuel cells and analytical sensors, Nano Today 6 (2011) 240–264.
[3] N.T.K. Thanh, L.A.W. Green, Functionalization of nanoparticles for biomedical applications, Nano Today 5 (2010) 213–230.
[4] Z. Nie, A. Petukhova, E. Kumacheva, Properties and emerging applications of self-assembled structures made from inorganic nanoparticles, Nat. Nanotechnol. 5 (2010) 15–25.
[5] M.H. Tu, T. Sun, K.T.V. Grattan, Optimization of gold-nanoparticle-based optical fiber surface plasmon resonance (SPR)-based sensors, Sens. Actuators B. 164 (2012) 43–53.
[6] F. Terzi, C. Zanardi, B. Zanfrognini, L. Pigani, S. Seeber, Z. Lukkari, T. Aaritalo, J. Kankare, Preparation and characterization of a redox multilayer film containing Au nanoparticles, J. Phys. Chem. C 113 (2009) 4868–4874.
[7] J.P. Chapel, J.F. Barret, Versatile electrostatic assembly of nanoparticles and polyelectrolytes: Coating, clustering and layer-by-layer processes, Curr. Opin. Colloid Interface Sci. 17 (2012) 97–105.
[8] N. Du, H. Zhang, D. Yang, One-dimensional hybrid nanostructures: synthesis via layer-by-layer assembly and applications, Nanoscale 18 (2012) 5517–5526.
[9] J.F. Hicks, Y. Seok-Shon, R.W. Murray, Layer-by-Layer growth of polymer/nanoparticle films containing monolayer-protected gold clusters, Langmuir 18 (2002) 2288–2294.
[10] J. Dhar, S. Patil, Self-assembly and catalytic activity of metal nanoparticles immobilized in polymer membrane prepared via layer-by-layer Approach, ACS Appl. Mater. Interfaces 4 (2012) 1803–1812.
[11] F. Zhang, M.P. Srinivasan, Layer-by-layer assembled gold nanoparticle films on amine-terminated substrates, J. Colloid Interface Sci. 319 (2008) 450–456.
[12] W. Yuan, C.M. Li, Direct modulation of localized surface plasmon coupling of Au nanoparticles on solid substrates via weak polyelectrolyte-mediated layer-by-layer self assembly, Langmuir 25 (13) (2009) 7578–7585.
[13] X. Sun, C. Zhai, X. Wang, Gold nanoparticles/chitosan dual-layer membranes modified acetylcholinesterase biosensor, Sens. Transducers J. 137 (2012) 226–234.
[14] M.V. Bracamonte, S. Bollo, P. Labbé, G.A. Rivas, N.F. Ferreyra, Quaternized chitosan as support for the assembly of gold nanoparticles and glucose oxidase: Physicochemical characterization of the platform and evaluation of its biocatalytic activity, Electrochim. Acta. 56 (2011) 1316–1322.
[15] N. Ferreyra, L. Coche-Guérente, J. Fatisson, M. Lopez Teijelo, P. Labbé, Layer-by-layer self-assembled multilayers of redox polyelectrolytes and gold nanoparticles, Chem. Commun. (2003) 2056–2057.
[16] N.F. Ferreyra, S. Bollo, G.A. Rivas, Self-assembled multilayers of polyethylenimine, DNA and gold nanoparticles. A study of electron transfer reaction, J. Electroanal. Chem. 638 (2010) 262–268.
[17] K. Rajesh, B. Sreedhar, T.P. Radhakrishnan, Assembly of gold nanoparticles on a molecular ultrathin film: Tuning the surface plasmon resonance, Chem. Phys. Phys. Chem. 11 (2010) 1780–1786.
[18] S.K. Ghosh, T. Pal, Interparticle coupling effect on the surface plasmon resonance of gold nanoparticles: from theory to applications, Chem. Soc. Rev. 107 (2007) 4797–4862.
[19] A. Sungsook, Y.J. Sung, K.K. Hae, A. Sambasivan, S.J. Lee, Polymeric self-assembly changes by surface-modified and in-situ-grown nanoparticles, Polymer 54 (2013) 1004–1009.
[20] S.C. Jiang, V. Markutsya, V. Tsukruk, Collective and individual plasmon resonances in nanoparticle films obtained by spin-assisted layer-by-layer assembly, Langmuir 20 (2004) 882–890.
[21] S.A. Miscoria, J. Desbrieres, G.D. Barrera, P. Labbé, G.A. Rivas, Glucose biosensor based on the layer-by-layer self assembling of glucose oxidase and chitosan derivatives on a thiolated gold surface, Anal. Chim. Acta 578 (2006) 137–144.
[22] I. Horcas, R. Frenández, J.M. Gómez-Rodriguez, J. Colchero, J. Gómez-Herrero, A.M. Baro, WSXM: A software for scanning probe microscopy and a tool for nanotechnology, Rev. Sci. Instrum. 78 (2007) 013705–013713.
[23] N.F. Ferreyra, E.S. Forzani, M. López Teijelo, L. Coche-Guérente, P. Labbé, Unraveling the spatial distribution of immunoglobulin, enzymes and polyelectrolytes within layer-by-layer self-assembled multilayers, Ellipsometric studies, Langmuir 21 (2006) 8931–8938.
[24] H. Fujiwara, Spectroscopic ellipsometry: Principles and applications, J. Wiley & Sons, United States, 2007.
[25] H.G. Tompkins, E.A. Irene (Eds.), Handbook of ellipsometry, William Andrew Publishing, New York, 2005.
[26] M. Losurdo, K. Hingerl (Eds.), Ellipsometry at the Nanoscale, Springer, Berlin Heidelberg, 2013.
[27] K. Haberska, T. Ruzgas, Polymer multilayer film formation studied by in situ ellipsometry and electrochemistry, Bioelectrochem. 76 (2009) 153–161.
[28] J. Zhou, D. Mu, H. Song, X. Leng, Y. Meng, W. Han, J. Yang, X. Di, Q. Chang, Plasmon resonances in nanoparticle system consisting of different materials, Opt. Commun. 295 (2013) 235–238.
[29] K.L. Kelly, E. Coronado, L.L. Zhao, G.C. Schatz, The Optical Properties of Metal Nanoparticles: The Influence of Size, Shape, and Dielectric Environment, J. Phys. Chem. B 107 (2003) 668.
[30] I.E. Sendroiu, S.F.L. Mertens, D.J. Schiffrin, Plasmon interactions between gold nanoparticles in aqueous solution with controlled spatial separation, Phys. Chem. Chem. Phys. 8 (2006) 1430–1436.
[31] C. Wang, H. Itoh, Evaluation of errors in the measurement of surface roughness at high spatial frequency by atomic force microscopy on a thin film, Jpn. J. Appl. Phys. 51 (2012), 08KB11-5.
[32] H.L. Zhang, S.D. Evans, J.R. Henderson, Spectroscopic ellipsometric evaluation of gold nanoparticle thin films fabricated using layer-by-layer self-assembly, Adv. Mater. 15 (2003) 531–534.
[33] E.S. Kooij, H. Wormeester, E.A. Martijn Brouwer, E. van Vroonhoven, A. van Silfhout, B. Poelsema, Optical characterization of thin colloidal gold films by spectroscopic ellipsometry, Langmuir 18 (2002) 4401–4413.
[34] Z. Qi, I. Honma, M. Ichihara, H. Zhou, Layer-by-layer fabrication and characterization of gold-nanoparticle/myoglobin nanocomposite films, Adv. Funct. Mater. 16 (2006) 377–386.
[35] X.J. Jeon, V. Panchagnula, J. Pan, A.V. Dobrynin, Molecular Dynamics simulations of mutilayer films of polyelectrolytes and nanoparticles, Langmuir 22 (2006) 4629–4637.
[36] A. Bonanni, M. Pumera, Y. Miyahara, Influence of gold nanoparticle size (2-50 nm) upon its electrochemical behavior: an electrochemical impedance spectroscopic and voltammetric study, Phys. Chem. Chem. Phys. 13 (2011) 4980–4986.
[37] A.J. Bard, L.R. Faulkner, Electrochemical methods. Fundamentals and applications, Jonh Wiley & Sons, United States, 2001.
[38] J.-N. Chazalviel, Ph. Allongue, On the Origin of the Efficient Nanoparticle Mediated Electron Transfer across a Self-Assembled Monolayer, JACS 133 (2011) 762–764.
[39] A. Barfidokht, S. Ciampi, E. Luais, N. Darwish, J.J. Gooding, The Influence of Organic-Film Morphology on the Efficient Electron Transfer at Passivated Polymer-Modified Electrodes to which Nanoparticles are Attached, ChemPhysChem 14 (2013) 2190–2197.
[40] A. Barfidokht, S. Ciampi, E. Luais, N. Darwish, J.J. Gooding, Distance-Dependent Electron Transfer at Passivated Electrodes Decorated by Gold Nanoparticles, Anal. Chem. 85 (2013) 1073–1080.
[41] J.B. Shein, L.M.H. Lai, P.K. Eggers, M.N. Paddon-Row, J.J. Gooding, Formation of efficient electron transfer pathways by adsorbing gold nanoparticles to self-assembled monolayer modified electrodes, Langmuir 25 (2009) 11121–11128.
[42] C.R. Bradbury, J. Zhao, D.J. Fermin, Distance-independent charge-transfer resistance at gold electrodes modifies by thiol monolayers and metal nanoparticles, J. Phys. Chem. C 112 (2008) 10153–10160.
[43] B. Ballarin, M.C. Cassani, E. Scavetta, D. Tonelli, Self-assembled gold nanoparticles modified ITO electrodes: The monolayer binder molecule effect, Electrochim. Acta 53 (2008) 8034–8044.
[44] J. Zhao, C.R. Bradbury, D.J. Fermin, Long-range electronic communication between metal nanoparticles and electrode surfaces separated by polyelectrolyte multilayer films, J. Phys. Chem. C 112 (2008) 6832–6841.